

**DIRECT QUANTIFICATION OF SOLUTE DIFFUSIVITY IN STRAINED
POROUS, VISCOELASTIC MATERIALS USING CORRELATION
SPECTROSCOPY**

by

Janty Shoga

A thesis submitted to the Faculty of the University of Delaware in partial fulfillment of the requirements for the degree of Master of Science in Biomechanics and Movement Science

Summer 2016

© 2016 Janty Shoga
All Rights Reserved

ProQuest Number: 10192780

All rights reserved

INFORMATION TO ALL USERS

The quality of this reproduction is dependent upon the quality of the copy submitted.

In the unlikely event that the author did not send a complete manuscript and there are missing pages, these will be noted. Also, if material had to be removed, a note will indicate the deletion.



ProQuest 10192780

Published by ProQuest LLC (2016). Copyright of the Dissertation is held by the Author.

All rights reserved.

This work is protected against unauthorized copying under Title 17, United States Code
Microform Edition © ProQuest LLC.

ProQuest LLC.
789 East Eisenhower Parkway
P.O. Box 1346
Ann Arbor, MI 48106 - 1346

**DIRECT QUANTIFICATION OF SOLUTE DIFFUSIVITY IN STRAINED
POROUS, VISCOELASTIC MATERIALS USING CORRELATION
SPECTROSCOPY**

by

Janty Shoga

Approved: _____
Christopher Price, Ph.D.
Professor in charge of thesis on behalf of the Advisory Committee

Approved: _____
Charles Swanik, Ph.D.
Director of the Biomechanics and Movement Science Program

Approved: _____
Kathleen Matt, Ph.D.
Dean of the College of Health Sciences

Approved: _____
Ann L. Ardis, Ph.D.
Senior Vice Provost for Graduate and Professional Education

ACKNOWLEDGMENTS

I would like to express my sincere appreciation to my advisor, Dr. Christopher Price, for the opportunity to work in his lab. I've grown a lot as a scientist and as a person throughout my time in the lab, and that would not have been possible without Professor Price's guidance.

I would also like to thank my lab mates, colleagues, and friends for their support and for their input in writing this thesis. Michael David for his willingness to challenge assumptions and his inspiring passion for research. Brian Graham for his camaraderie in developing image processing techniques and code to make our research possible. Melanie Smith for setting such high standards for working in a lab, and for helping me transition into a biology lab by being so knowledgeable and helpful. Lastly, Omar Banda for offering a different perspective on my work and for lending an ear whenever I had an idea.

I would also like to acknowledge Dr. Jeffrey Caplan, Dr. Chandran Sabanayagam, and Michael Moore at the Delaware Biotechnology Institute's Bioimaging Center for teaching me how to use the confocal microscopes and perform the techniques that were necessary to conduct the research in this thesis.

Finally, I must thank my parents and family for their support and encouragement throughout my life, and especially during the completion of this thesis. I could not have done this without them.

TABLE OF CONTENTS

LIST OF FIGURES.....	v
ABSTRACT.....	viii
Chapter	
1 INTRODUCTION	1
2 METHODS	6
2.1 Correlation Spectroscopy Theory and Analysis	6
2.1.1 Fluorescence Correlation Spectroscopy	6
2.1.2 Raster Image Correlation Spectroscopy	9
2.2 Sample Preparation	12
2.2.1 Agarose Plugs.....	12
2.2.2 Bovine Articular Cartilage	12
2.3 Imaging.....	13
2.4 Acquisition of Correlation Spectroscopy Data	13
2.5 Statistical Analysis	16
3 RESULTS	17
3.1 Agarose.....	17
3.2 Cartilage	20
4 DISCUSSION	25
REFERENCES	32
Appendix	
A SUPPLEMENTAL INFORMATION	43

LIST OF FIGURES

- Figure 1: **(A)** Example of a 1-second subset of fluorescent fluctuation data from a representative FCS trial of 10 nM FITC in aqueous solution **(B)** Semi-log graph of the autocorrelation output from the data in A, and the best fit of the data to the full form FCS diffusion model, including terms for triplet state kinetics (Equation 3). 8
- Figure 2: **(A)** Representative image from RICS data set that captures the ‘slow’ diffusive movement of 200 nm fluorescent particles in an aqueous solution. Due to the raster-scanning of the spatially over-sampled point spread function, these slowly diffusing ‘point-source’ fluorescent particles appear as streaks in both the x- and y-scan directions. **(B)** Average autocorrelation surface from RICS data (images) of 200 nm fluorescent particles diffusion in an aqueous solution. **(C)** Representative image from RICS data of the faster diffusive movement of aqueous 10 nM FITC. **(D)** Average autocorrelation surface from RICS data (images) of aqueous 10 nM FITC. 11
- Figure 3: Diffusion coefficients of FITC, 3K dextran, and 10K dextran, as determined by FCS and RICS in aqueous solutions and various concentrations of agarose (% wt/vol). Data reported as mean + SD. Bars indicate significant difference ($p < 0.05$, one-way ANOVA with Tukey post-hoc test) in diffusivity between different sized solutes for a given agarose concentration and detection technique. Letters indicate significant difference in solute diffusivity (e.g. FITC, 3k-, or 10k-dextran) between agarose concentrations for a given solute and detection technique; a = significant different then corresponding solute values at 0% (aqueous solution), b = 1% agarose, c = 3% agarose, and d = 5% agarose ($p < 0.05$, one-way ANOVA, Tukey post-hoc test). No significant differences in diffusivity were observed among quantification methods for any given combination of solute size and agarose concentration ($p < 0.05$, paired t-test). These results demonstrate the solute diffusivity in agarose is inversely related to solute size and gel density. 18

Figure 4: Diffusion coefficients of 3K dextran determined by FCS and RICS in 1% agarose at 0% and 10% compressive strain. Data reported as mean + SD. Bars indicate significant difference in diffusivity among uncompressed agarose plugs and plugs compressed to 10% strain ($p < 0.05$, paired t-test, $n = 5$ for each group). These data show that strain affects the diffusion coefficient of 3K dextran in 1% agarose, and while the diffusion coefficients obtained via RICS were not significantly different, there does seem to be a trend towards significance ($p=0.0535$)..... 19

Figure 5: XY-scatter plot of paired FCS and RICS diffusivity measures for FITC, 3K dextran, and 10K dextran under the various experimental conditions tested (e.g. 0, 1, 3, and 5% agarose at 0% and 10% compressive strains). Individual data points for each tested condition are displayed. The linear regression line, as shown by the solid grey line was fit to the data set encompassing all conditions; $y = 0.9377x + 25.49$, 95% confidence intervals of the fit are shown by the dotted grey lines, $R^2 = 0.9469$, $p < 0.0001$. The slope and R^2 value being nearly equal to 1 demonstrates the repeatability of diffusivity measurements made by FCS and RICS. 20

Figure 6: Diffusion coefficients of 3K dextran in the superficial, middle, and deep zones of bovine calf cartilage under 0, 10, 20, and 30% strains as determined by FCS (A) and RICS (B). While there was a trend toward decreasing 3k-dextran diffusivity with the application of 10% strain to the superficial layer under both techniques no significant differences were found between experimental groups ($p > 0.05$, One-way ANOVA, Tukey post-hoc and paired t-test, as applicable). Data reported as mean + SD ($n = 12$ for each group). While there were no significant differences in this data, there may be a slight decreasing trend in the diffusion coefficient of 3K dextran between 0% and 10% strain superficial zone cartilage. 22

Figure 7: Diffusion coefficients of FITC and 3K dextran as determined by FCS (A) and RICS (B) in the superficial, middle, and deep zones of uncompressed bovine calf cartilage. No significant differences were found between experimental groups ($p > 0.05$, One-way ANOVA, Tukey post-hoc and paired t-test, as applicable). Data reported as mean + SD ($n = 6$ for each group). While there were no significant differences in this data, there may be a slight decreasing trend between the diffusion coefficients of FITC and 3K dextran in superficial zone cartilage; no trend is apparent in the middle and deep zone cartilage. 23

- Figure 8: XY-scatter plot of diffusion coefficient values of 3K dextran and FITC in all cartilage zones, at all applied strains obtained by RICS versus those obtained by FCS. Data points denote the average diffusion coefficient across three locations within a sample. The linear regression line is shown by a solid grey line ($y = 0.5450x + 7.671$), with 95% confidence intervals shown by dotted grey lines. Significant correlation was found ($p < 0.0001$), $R^2 = 0.1820$. The low slope and R^2 values indicate low repeatability in quantifying the diffusion coefficient of 3K dextran in cartilage using FCS and RICS, perhaps due to the spatial heterogeneity in cartilage matrix structure..... 24
- Figure A.1: **(A)** Example of a 10-second FCS trial that has spurious peaks much higher than the rest of the dataset. Such peaks are typically indicative of an aggregate of fluorescent solute particles, and the 10-second trial in which such peaks occurred were excluded from the diffusion analysis. **(B)** The autocorrelation and model fit of representative data containing an aggregate of fluorescent particles data. The presence of the aggregate results in a second, superimposed “hump” in the autocorrelation, indicative of a second solute species being present in the observation volume. **(C)** Example of a 10-second FCS trial in which photobleaching of the fluorescent particles (typically of an immobile fraction) has occurred. The photobleaching effect manifests in an exponentially decaying photon count rate. Any 10-second trials in which photobleaching effects were seen were removed from the diffusion analysis. **(D)** The autocorrelation and model fit of representative data exhibiting time-dependent photobleaching. Notice the drastically delayed decay time due to the contribution of the slow photobleaching kinetics..... 43
- Figure A.2: These are images of DAPI-stained cell nuclei in the superficial **(A)**, middle **(B)**, and deep **(C)** zones of a cartilage plug. These images were taken at 20X magnification, under 405 nm laser light exposure. These images demonstrate the heterogeneity in cellularity between the superficial and middle and deep zones. When performing FCS and RICS analyses, we avoided taking diffusion measurements within a cell. However, due to the increased cellularity in the superficial zone, this was not always achievable for every sample. The red boxes and red dots represent the sizes of the RICS and FCS observation regions, respectively..... 44

ABSTRACT

Articular cartilage is an avascular tissue, and as such, diffusive transport is important in cartilage homeostasis and disease. While numerous techniques have been used to quantify diffusivity within porous, hydrated tissues, and to assess both cartilage pathology and the maturity of tissue engineered constructs, to date, these techniques have suffered from limitations in terms of their invasiveness and spatial resolution. In the present study, we implemented and compared two separate correlation spectroscopy techniques, fluorescence correlation spectroscopy (FCS) and raster image correlation spectroscopy (RICS), for quantifying fluorescent solute diffusion in agarose and articular cartilage. Specifically, we observed the equilibrium diffusion of fluorescein isothiocyanate (FITC), and Alexa Fluor 488-conjugated 3K and 10K dextrans in aqueous solutions, agarose gels of varying concentration (1%, 3%, 5%), and in different zones of juvenile bovine articular cartilage explants (i.e. superficial, middle, and deep). In agarose, diffusion coefficients were inversely related to the size of the molecule and agarose gel concentration. In cartilage, no statistically significant trends were observed; however, the diffusion coefficient values obtained via FCS and RICS were in agreement with previously published work, using other techniques. Thus, this study demonstrated the utility of FCS and RICS as simple and minimally invasive ways to quantify solute diffusivity within both agarose constructs and bovine articular cartilage explants.

Chapter 1

INTRODUCTION

Articular cartilage is a highly hydrated tissue whose primary function is to facilitate load-bearing and low-friction motion between joint surfaces. Articular cartilage is composed primarily of water (approximately 60-85% wet weight), and this water plays a critical role in the tissue's function [1-4]. The remainder of the tissue consists of collagen (predominantly type II, 15-20% wet weight), proteoglycan (~5%), and a small percentage of non-collagenous proteins and glycoproteins [5]. Within articular cartilage, collagen contributes to the tissue's tensile stiffness, while the negatively-charged proteoglycans are essential for cartilage's characteristic swelling and water retention [6]. Together, the collagens and proteoglycans in articular cartilage form a stiff, hydrated, fiber-reinforced solid matrix that serves as a scaffold for specialized cartilage cells, chondrocytes [5]. Chondrocyte, collagen, and proteoglycan distributions are heterogeneous throughout the depth of the articular cartilage [7], resulting in varying solid-matrix and tissue hydration properties throughout the tissue [8-12].

Cartilage, and the chondrocytes embedded within it, rely on diffusion or load-induced convection of interstitial fluid to move solutes through the tissue since cartilage is avascular. The same is true of engineered cartilaginous tissue, such as those composed of naturally-derived hydrogels, e.g. agarose, alginate, hyaluronan, fibrin, or collagen [13-17]. Previous studies have demonstrated that dynamic loading of cartilage explants [18] and engineered cartilage constructs [16, 19, 20] can enhance

the transport of large macro-molecules into/through cartilage via convective processes. However, it is generally believed that diffusion is the predominant transport mechanism governing the distribution/exchange of smaller nutrients, waste, and signaling molecules in cartilaginous tissues [21]. As a result, molecular diffusion would be expected to play a critical role in the regulation of cartilage homeostasis and health, and in the maturation of engineered cartilage tissues.

Diffusivity within porous materials is dependent upon several properties of the diffusing solute and the extracellular matrix, such as the size and geometry of the solute and matrix pores. Within cartilage, the pore size is predicted to range from 2 to 6 nm, and has been found to be dependent upon the composition, structure, hydration, and degree of matrix compaction [22]. Thus, alterations in tissue composition and hydration, such as those related to depth- and age-dependent changes in tissue ultrastructure, disease-state, and mechanical loading, have the ability to influence the diffusive transport of solutes required for regulating chondrocyte metabolism, homeostasis, and health in natural and engineered cartilage tissues. Consequently, quantification of diffusivity within these tissues is an important tool for studying the transport of molecules within cartilage, as well as their natural physiology.

Various imaging techniques have been used to quantify solute diffusivity within cartilaginous tissues. Magnetic resonance imaging (MRI) techniques, such as diffusion weighted [23] and diffusion tensor MRI [24-30], and NMR spectroscopy [31-34] have been used successfully to quantify diffusion and diffusional anisotropy within cartilage [35, 36]. However, they are restricted to the study of ions and very small molecules [23, 24, 28, 29, 31], and have limited spatial resolution compared to cartilage's micro-scale features [37, 38]. They also typically require long imaging

times, and can be costly [39]. Adsorption/desorption diffusion assays can be implemented within cartilage through a variety of fairly simple quantification strategies, including optical/fluorescent imaging; however, such assays only report bulk diffusion measures within a tissue and thus lack spatial specificity. Conversely, fluorescence recovery after photobleaching (FRAP) is a fairly straightforward and widely-implemented microscopy technique that enables the quantification of micro-scale diffusion within cells and tissues. Numerous studies using photobleaching techniques have quantified solute diffusion within the context of engineered cartilage constructs [9], cartilage explants [9, 40], in situ calcified cartilage [41, 42], and growth plate cartilage [43]. However, despite the ubiquity of its application, quantification of diffusivity via FRAP is not without its limitations. FRAP analysis involves the application of an external perturbation, in the form of photobleaching, to quantify solute diffusivity. The FRAP technique requires specific assumptions, whose validity can affect the accuracy of the derived transport results, regarding the system being observed and the nature of the perturbation. These include: 1) knowledge of the geometric shape of the bleached region of interest (ROI), 2) instantaneous bleaching within the ROI, 3) a bleaching profile approximated as a radial step function, 4) a uniformly and isotropically bleached ROI, and 5) a restriction of in-plane diffusion [44, 45]. Additionally, FRAP requires the use of high laser intensities to induce photobleaching of a relatively concentrated (μM) fluorescent solute, which may have phototoxic effects on cells and tissues under observation [46]. However, other fluorescence microscopy-based, correlation spectroscopy techniques exist that are capable of quantifying solute diffusion while avoiding the limitations of FRAP.

Recently, fluorescence correlation spectroscopy (FCS) has been used to quantify the diffusivity of fluorescent solutes in healthy and chemically degraded porcine articular cartilage [47]. FCS is based upon the correlation analysis of fluctuations in fluorescence intensity driven by physical processes within the system under study. Unlike FRAP, FCS does not rely on large external perturbations to the system to study diffusive transport, but is instead based upon observation of small, intrinsically-driven perturbations/fluctuations in the system due to the Brownian motion of the particles under study. FCS is a well-developed and highly-sensitive analytical tool that represents an alternative methodology for quantifying solute transport within articular cartilage. Advantages of FCS over other quantification methods include its femto-scale observation region, well-defined and consistent data collection and analysis methodologies, and very short experiment times (~1 minute). Additionally, FCS does not require high laser powers for data collection, and is suitable for low (nanomolar) solute concentrations. However, FCS is not an image-based technique, so the observation region cannot be directly visualized while collecting data and average diffusivity measurements are restricted to the stationary location of the observation volume. A recently developed image-based extension of FCS, called raster image correlation spectroscopy (RICS) [48, 49], allows for the quantification of solute diffusion within raster-scanned, confocal images, and may thus prove useful for measuring solute diffusion in engineered and natural cartilage tissues. However, no studies have been conducted in which RICS has been applied to the quantification of solute diffusion within porous, engineered or natural cartilage materials. Thus, the goals of the present study were to apply and compare FCS and

RICS in quantifying the solute diffusion in various agarose constructs and in compressively strained bovine articular cartilage explants.

Chapter 2

METHODS

2.1 Correlation Spectroscopy Theory and Analysis

In the present study, solute diffusivity was quantified via both fluorescence correlation spectroscopy (FCS) and raster image correlation spectroscopy (RICS), using adaptations of protocols previously described in the literature [50-52]. FCS is an Eulerian measurement technique that measures fluorescent intensity fluctuations due to transits of fluorescent solutes through a small (~ 1 -fL) observation volume. RICS is an image-based extension of FCS that exploits the time lags between consecutively and dynamically captured pixels (observation volumes) in a raster-scanned image to capture the diffusion of fluorescent solutes over time. The theory behind FCS and RICS diffusivity measurement and their application are described briefly herein.

2.1.1 Fluorescence Correlation Spectroscopy

FCS is a microscopy technique that is dependent upon the use of a small, well defined, and fixed observation volume (achieved using confocal microscopy) [50, 53, 54]. When low-concentration fluorophores (< 10 nM) transit this stationary observation volume, fluctuations in fluorescence intensity, detected by optical detectors are recorded (Figure 1). Temporal autocorrelation analysis (Equation 1), which represent the correlation of a time series against itself after having been shifted by a time lag, τ , is performed on the intensity traces to extract information regarding the physics underlying the observed fluctuations according to:

$$g(\tau) = \frac{\langle \delta I(t) \delta I(t + \tau) \rangle}{\langle I(t) \rangle^2} \quad (1)$$

where $I(t)$ represents the recorded fluorescence intensity and $\delta I(t) = I(t) - \langle I(t) \rangle$ is the deviation from the mean intensity. The brackets denote averaging across all data collected (Equation 2),

$$\langle \delta I \rangle = \frac{1}{M} \sum_{i=1}^M (I_i - \langle I \rangle) \quad (2)$$

where M is the total number of data points collected. When analyzed with an appropriate physical model, quantitative information regarding diffusion coefficients, concentrations, chemical reaction rates, and particle photophysics can be obtained from the autocorrelation output.

To extract measures of diffusivity from the autocorrelation output, autocorrelation curves were fit to a normal diffusion model (Equation 3) [55] that considers the parameters of the imaging system, but does not require any assumptions to be made about the system being observed (e.g. sample geometry).

$$G(\tau) = G(0) \left(\frac{1}{1 + \tau/\tau_D} \right) \left(\frac{1}{1 + \tau/a^2\tau_D} \right)^{1/2} + G(\infty) \quad (3)$$

Where $G(0) = 1/N$ gives the inverse of the mean number of diffusing particles in the observation volume over time, τ_D is the characteristic solute residence time within the observation volume, and $a = \omega_z/\omega_0$ is the ratio of the axial (ω_z) to radial (ω_0) waists (e^{-2} radii) of the observation volume. The dimensions of the axial and radial waists of the observation volume are established by the optical equipment and the wavelength of the emitted light, and are described mathematically by the microscope's point spread function (PSF). Typically, the PSF is ellipsoid in shape with ω_0 ranging from 200-300 nm and $\omega_z \approx 3-5\omega_{xy}$ [51, 57, 58]. In FCS measurements, values for ω_0 and a can be quantified empirically from confocal scans of point-

emitting sources, or via calibration, by performing FCS on a solute with a known diffusion coefficient (see below).

In our FCS analysis, a triplet state term was included in the model to account for fluorescent particle blinking due to entering the triplet state. Equation 4 is the full form of the FCS diffusion model, including terms for triplet state kinetics.

$$G(\tau) = G(0) \left(\frac{1 - F + F e^{-\tau/\tau_F}}{1 - F} \right) \left(\frac{1}{1 + \tau/\tau_D} \right) \left(\frac{1}{1 + \tau/a^2\tau_D} \right)^{1/2} + G(\infty) \quad (4)$$

Where F is the fraction of fluorescent molecules in the triplet state and τ_F is the triplet state relaxation time. Lastly, the characteristic residence time (τ_D), determined via one-photon excitation is related to the diffusion coefficient and is described by Equation 5.

$$D = \frac{\omega_0^2}{4\tau_D} \quad (5)$$

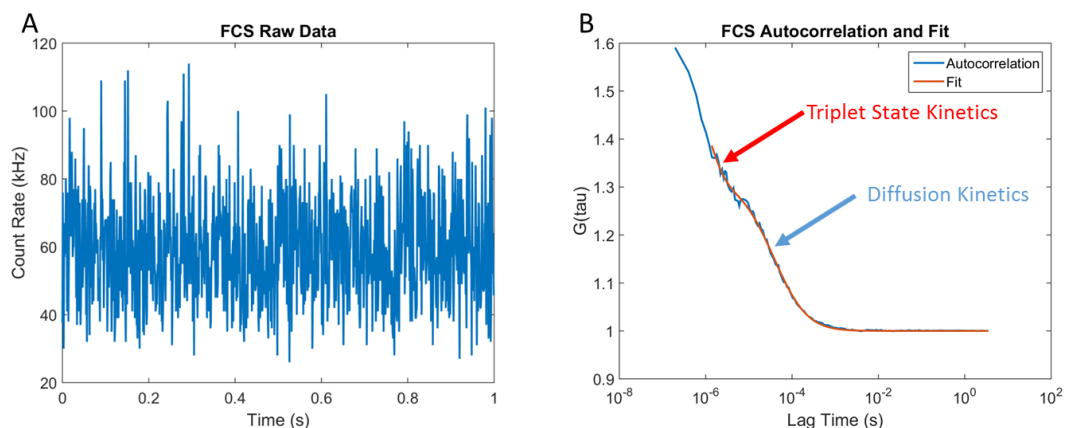


Figure 1: (A) Example of a 1-second subset of fluorescent fluctuation data from a representative FCS trial of 10 nM FITC in aqueous solution (B) Semi-log graph of the autocorrelation output from the data in A, and the best fit of the data to the full form FCS diffusion model, including terms for triplet state kinetics (Equation 3).

2.1.2 Raster Image Correlation Spectroscopy

Similar to FCS, RICS is a fluorescence microscopy technique that is dependent upon the use of a small, well-defined observation volume; however, unlike in FCS, the observation volume does not remain fixed. Instead, a dynamic pattern of observation is generated using a laser scanning confocal microscope (LSCM), which raster-scans the confocal observation volume through space to capture images pixel-by-pixel. Because of the raster-scanning procedure, images from LSCMs contain a hidden spatial and temporal structure. RICS exploits this structure, or more specifically the defined time lag between consecutively captured pixels and lines to quantify the diffusivity of solutes within the images [59].

Prior to RICS analysis, background subtraction is performed to remove immobile particles from the image data sets using previously published methodologies [59]. Then two-dimensional spatial autocorrelation is performed on each background-subtracted image to extract the kinetics of solute diffusion from within the collected images. Spatial autocorrelation is the correlation of an image against itself after having been shifted by a spatial increment ξ and ψ in the x and y directions, respectively, and can be represented as a function of ξ and ψ by Equation 6.

$$G(\xi, \psi) = \frac{\langle \delta I(x, y) \delta I(x + \xi, y + \psi) \rangle}{\langle I(x, y) \rangle^2} \quad (6)$$

Again, where $I(x, y)$ represents the recorded fluorescence intensity and $\delta I(x, y) = I(x, y) - \langle I(x, y) \rangle$ is the deviation from the mean intensity. This 2-dimensional spatial correlation is efficiently computed using fast Fourier transform (FFT) techniques.

To extract the kinetics of diffusion from the data, the resultant autocorrelation output (surface) is fit to a normal diffusion model [56] that considers both the raster scan parameters of the imaging system and the physics of diffusion; thus, allowing one

to account for the relationship between time and the position of the LSCM scanning beam while not requiring any assumptions to be made about the system being observed (e.g. sample geometry) to determine diffusivity.

The contribution of the raster scanning pattern of the confocal microscope to the autocorrelation of the images is described by Equation 7.

$$S(\xi, \psi) = \exp\left(-\left(\frac{1}{2}\left[\left(\frac{2\xi\delta r}{\omega_0}\right)^2 + \left(\frac{2\psi\delta r}{\omega_0}\right)^2\right]\right)\left(1 + \frac{4D(\tau_p\xi + \tau_l\psi)}{\omega_0^2}\right)^{-1}\right) \quad (7)$$

Where x is the horizontal pixel position, y is the vertical pixel position, δr is the pixel size, ω_0 is the radial waist dimension of the PSF, D is the diffusion coefficient, τ_p is the pixel dwell time, and τ_l is the line scan time. The pixel size must be 3-4 times smaller than the radial waist of the PSF to achieve a requisite spatial oversampling of the PSF [48, 51]. Further, the pixel dwell time must be optimized for the system being observed such that the speed of diffusion is on approximately the same time scale as the speed of scanning [49]. Quickly diffusing particles are best observed at short pixel dwell times (fast scan speeds), while slowly diffusing particles should be observed at longer pixel dwell times (slower scan speeds).

The contribution of particle diffusion to the autocorrelation of the images is described by Equation 8.

$$G(\xi, \psi) = \frac{\gamma}{N} \left(1 + \frac{4D(\tau_p\xi + \tau_l\psi)}{\omega_0^2}\right)^{-1} \left(1 + \frac{4D(\tau_p\xi + \tau_l\psi)}{\omega_z^2}\right)^{-1/2} \quad (8)$$

Where γ is a factor that describes the geometry of the illumination volume (and equals 0.35 for a 3D Gaussian [52]), N is the mean number of diffusing particles in the observation volume over time, and ω_z is the axial waist dimension of the PSF. Again, the ellipsoidal PSF dimensions share the relationship $\omega_z \approx 3-5\omega_0$ for one-photon

confocal microscopy [57, 58], and ω_0 and ω_z can be quantified by performing RICS on a solute with a known diffusion coefficient. Finally, the autocorrelation of the images is described by the product of the functions, as in Equation 9.

$$G_s(\xi, \psi) = S(\xi, \psi) \times G(\xi, \psi) \quad (9)$$

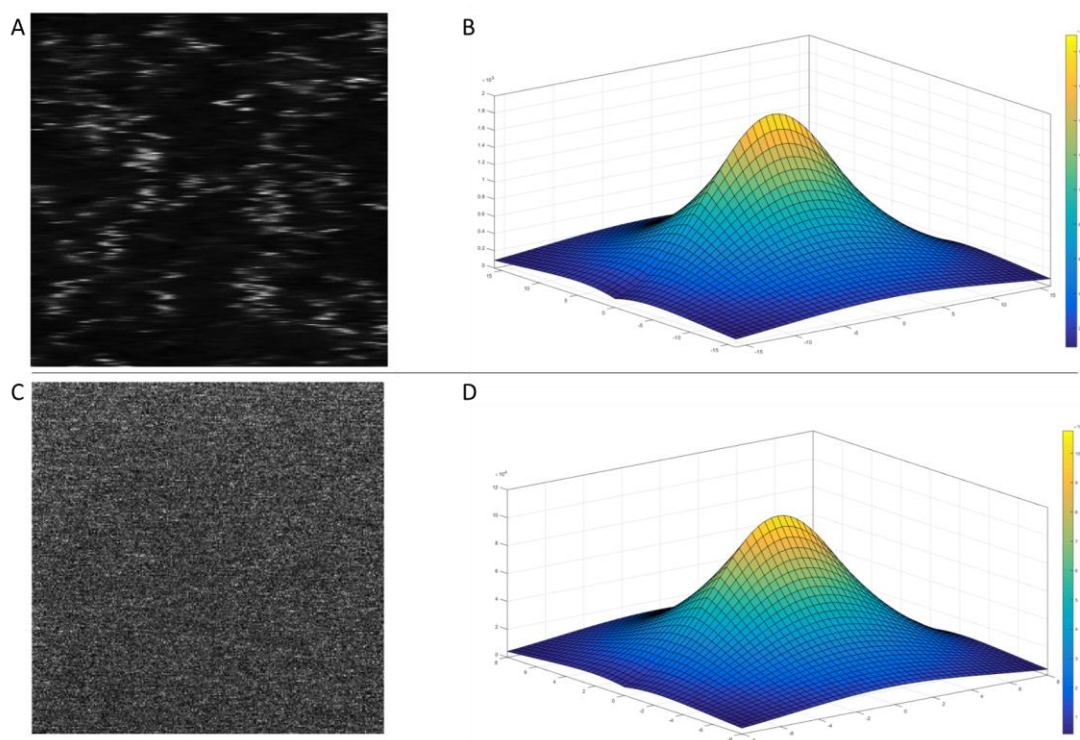


Figure 2: **(A)** Representative image from RICS data set that captures the ‘slow’ diffusive movement of 200 nm fluorescent particles in an aqueous solution. Due to the raster-scanning of the spatially over-sampled point spread function, these slowly diffusing ‘point-source’ fluorescent particles appear as streaks in both the x- and y-scan directions. **(B)** Average autocorrelation surface from RICS data (images) of 200 nm fluorescent particles diffusion in an aqueous solution. **(C)** Representative image from RICS data of the faster diffusive movement of aqueous 10 nM FITC. **(D)** Average autocorrelation surface from RICS data (images) of aqueous 10 nM FITC.

2.2 Sample Preparation

2.2.1 Agarose Plugs

Agarose (MP Biomedical, Cat. No. 02193983) plugs were prepared at densities of 1, 3, and 5% w/v in water. Briefly, melted agarose gel was cast into a 1.5 mm-thick slab between glass slides and solidified at 4°C for at least 30 minutes. Once solidified, 3 mm-diameter plugs (n = 55) were prepared using a biopsy punch. Following isolation, plugs were equilibrated for 24 hours at 4°C in 10 nM solutions of either fluorescein isothiocyanate (FITC; MW = 389 Da; Sigma-Aldrich, Cat. No. F7250), AlexaFluor488-conjugated 3K dextran (AF488-3K; MW = 3,000 Da; Molecular Probes, Cat. No. D34682), or AF488-10K dextran (MW = 10,000 Da; Molecular Probes, Cat. No. D22910) in PBS.

2.2.2 Bovine Articular Cartilage

Intact, healthy joints from freshly slaughtered bovine calves (< 1-year-old; n = 3) were obtained from a local abattoir (Green Village Packing, Green Village, NJ). Upon receipt, full thickness articular cartilage plugs (3-mm diameter) were harvested from the medial femoral condyles, using a biopsy punch. Plugs were cut into 1 mm-thick sections (n = 35), and separated into groups corresponding to the superficial, middle, and deep zones. The first 1 mm-thick section corresponded to the tissue of the superficial zone; the subsequent section corresponded to the middle zone; and the deepest 1 mm-thick section absent subchondral bone corresponded to the deep zone. Following isolation, bovine plugs were stained with 2 μM DAPI (Molecular Probes, Cat. No. D1306) for 1 hour at 4°C, followed by 24-hour equilibration in 10 nM of fluorescein or AF488-3K Dextran to facilitate solute diffusion measurements.

2.3 Imaging

Agarose and articular cartilage plugs were imaged within in a custom-designed sample holder that incorporated modular spacers allowing the application of specified degrees of equilibrium strain (ex. 0, 10, 20, or 30% strain) in unconfined compression between an impermeable No. 1 coverslip and a glass slide. Samples were surrounded by their respective dye solutions to maintain hydration and a constant source of bathing solute during observation. Agarose plugs were sequentially compressed to 0% and 10% equilibrium strain, while cartilage plugs were sequentially compressed to 0%, 10%, 20%, and 30% equilibrium strain. Samples were allowed to equilibrate (effectively under stress-relaxation) for a minimum of 10-minutes following compression and prior to imaging; mechanical testing on similar samples confirmed that this length of time allowed full relaxation of both agarose and cartilage plugs in unconfined compression. Prior to performing correlation spectroscopy, reflected light imaging (using 633-nm excitation) was used to identify the plug/coverglass interface and to allow positioning of the observation volume/plane $\sim 20\text{-}\mu\text{m}$ into the sample. In addition, standard DAPI imaging was used to observe chondrocyte cell nuclei within the cartilage plugs and to insure that the FCS observation volume and center of RICS imaging region were placed in regions away from identifiable chondrocytes (Supplemental Figure 2).

2.4 Acquisition of Correlation Spectroscopy Data

FCS and RICS were each performed in a paired manner, at three different observation locations (separated by $\sim 40\text{-}\mu\text{m}$ from each other) within each agarose or cartilage specimen in order to obtain a single average diffusivity value for each sample and technique. All correlation spectroscopy data and images were collected on either a

Zeiss LSM780 or Zeiss LSM880 laser scanning confocal microscope, similarly equipped with FCS and RICS capabilities. For all tests, a 488-nm Argon laser, reflected off of a 488-nm primary dichroic, was used to excite the fluorescent solutes (FITC, AF488-3K dextran, or AF488-10K dextran) through a 40X water immersion lens (C-Apochromat 40x/1.20 W Korr M27). A spectral array of GaAsP detectors were utilized to collect emitted fluorescent light between 490 nm and 543 nm. For both FCS and RICS, the confocal pinhole size was set to 1 Airy Unit.

Prior to performing correlation spectroscopy, the PSF geometry (ω_0 and ω_z) of the LSCM was determined in both FCS and RICS imaging configurations using an aqueous solution containing solute of known diffusivity. In the present study, we used 10 nM fluorescein dissolved in water, assuming a reference diffusion coefficient of $450 \mu\text{m}^2/\text{s}$ [60-63]. The reference solution was imaged within a 9-mm diameter by 0.12-mm deep well (SecureSeal imaging spacers) behind a No. 1 cover glass. PSF geometry (typically $\omega_0 = 254 \pm 28$ nm and $\omega_z = 1.27 \pm 140$ nm) was determined by fitting the FCS or RICS autocorrelation data to diffusion models utilizing a fixed diffusion coefficient of $450 \mu\text{m}^2/\text{s}$. PSF calibration was performed daily following warm-up and stabilization of the microscope and laser. Once the PSF parameters were determined, FCS and RICS analyses was performed on samples such that the PSF parameters (ω_0 and ω_z) remained fixed, and the diffusivity parameter was varied to produce a best-fit to the autocorrelation.

Initial image collection settings for both FCS and RICS were established based upon published protocols [47-59, 64-72] and were subsequently optimized for the present study. The following procedures and settings were used for FCS. Prior to data collection the laser intensity was adjusted to achieve a count rate of $\sim 10,000$ Hz, and

confocal pin-hole alignment and objective correction was performed to maximize the number of photon-counts per second. Each FCS measurement consisted of the collection of ten consecutive, 10-second-long FCS data captures at a single observation location, encompassing $\sim 10^6$ to 10^8 individual transits of fluorescent solute through the FCS observation volume. Temporal autocorrelation of each 10-second trial was automatically performed by hardware on the microscope and recorded by the Zeiss software. Following collection, each FCS data trace and autocorrelation sequence was visualized. If significant photobleaching (Supplemental Figure 1a, typically only seen in the first 10-second capture), or fluorescent particle aggregation (Supplemental Figure 1b, evidenced as brighter, slower decaying intensity fluctuations) was observed within a specific 10-second trace, that trace was individually excluded from further analysis. An average autocorrelation curve was generated and fit to the full form diffusion model (Equation 4) from the remaining collection of 10-second trials in each 100-second dataset.

RICS experiments were performed immediately following each FCS data acquisition in the same sample location, using the same objective and excitation-emission settings as for FCS. Each RICS experiment was conducted at a spatially oversampled optical zoom (200X-320X; 50-80 nm pixel size), as required for RICS data collection and analysis. Between 50 and 100 images (frames) were captured for each test at a frame size of either 256 x 256- or 512 x 512-pixels. The pixel dwell time varied from 0.64 μ s to 12.6 μ s, resulting in line scan times between 0.77 ms and 7.56 ms, and frame rates between 0.52 fps and 2.55 fps. Following collection, RICS images were analyzed using a custom MATLAB (MathWorks) script to perform spatial autocorrelation on each raster-captured image and to fit the resultant autocorrelation

(averaged across all frames in a single test) to a diffusion model accounting for both solute diffusion and the raster scanning acquisition (Equations 6, 7, and 8).

2.5 Statistical Analysis

Repeated measures two-way ANOVA was performed separately on FCS and RICS data for the cartilage datasets and the unstrained agarose dataset. Repeated measures one-way ANOVA was performed on all datasets, with Tukey's multiple comparison post-hoc test to determine significant differences between groups. Correlation and linear regression analyses were also performed on agarose and cartilage datasets, separately, to compare the average diffusion coefficients obtained via FCS versus those obtained via RICS. All data are presented as mean \pm standard deviation (SD). All statistical analyses were performed using the GraphPad Prism statistical analysis software. For all tests, $p < 0.05$ indicated significance.

Chapter 3

RESULTS

3.1 Agarose

The diffusivity of various nanomolar concentration fluorescent solute species were quantified in aqueous solutions, as well as in agarose plugs under various compressive strains using both FCS and RICS techniques. In aqueous solution, the diffusivity of fluorescein, which was set to the reference values of $450 \mu\text{m}^2/\text{s}$ to establish the PSF geometry for both techniques, was, as expected, significantly greater than that of 3K dextran ($153.37 \pm 3.19 \mu\text{m}^2/\text{s}$, $p < 0.0001$; and $165.59 \pm 18.42 \mu\text{m}^2/\text{s}$, $p < 0.0001$, for FCS and RICS, respectively; one-way ANOVA, Tukey post-hoc) and 10K dextran ($112.99 \pm 2.71 \mu\text{m}^2/\text{s}$, $p < 0.0001$ and $108.34 \pm 12.88 \mu\text{m}^2/\text{s}$; $p < 0.0001$ one-way ANOVA, Tukey post-hoc) (Figure 3). The diffusion coefficient of 3K dextran, as determined by RICS, was also significantly greater than that of 10K dextran in aqueous solution ($p = 0.0002$ for RICS data, $p = 0.3449$ for FCS data, one-way ANOVA, Tukey post-hoc). No significant differences in aqueous diffusivity were observed between quantification techniques (FCS versus RICS) for a given solute size.

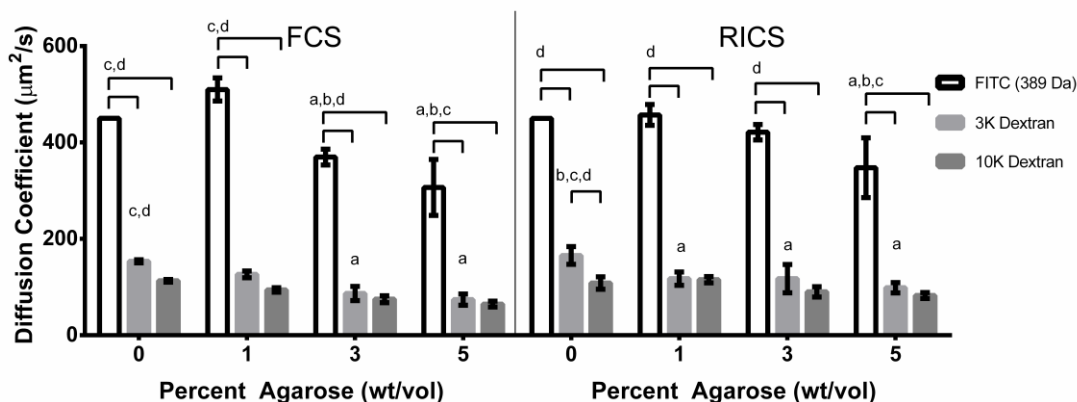


Figure 3: Diffusion coefficients of FITC, 3K dextran, and 10K dextran, as determined by FCS and RICS in aqueous solutions and various concentrations of agarose (% wt/vol). Data reported as mean \pm SD. Bars indicate significant difference ($p < 0.05$, one-way ANOVA with Tukey post-hoc test) in diffusivity between different sized solutes for a given agarose concentration and detection technique. Letters indicate significant difference in solute diffusivity (e.g. FITC, 3k-, or 10k-dextran) between agarose concentrations for a given solute and detection technique; a = significant different then corresponding solute values at 0% (aqueous solution), b = 1% agarose, c = 3% agarose, and d = 5% agarose ($p < 0.05$, one-way ANOVA, Tukey post-hoc test). No significant differences in diffusivity were observed among quantification methods for any given combination of solute size and agarose concentration ($p < 0.05$, paired t-test). These results demonstrate the solute diffusivity in agarose is inversely related to solute size and gel density.

Within agarose plugs it was observed that solute diffusivity, as measured by both FCS and RICS, was dependent upon agarose concentration, solute size, and applied compressive strain (Figures 3 and 4). For all solute species, diffusivity decreased with increasing agarose concentration ($p < 0.0001$, repeated measures two-way ANOVA, for both FCS and RICS datasets) (Figure 3) and with the application of 10% compressive strain (FCS: $p = 0.0127$, RICS: $p = 0.0535$; Figure 4). Similarly, for a given gel concentration diffusivity was inversely related to both solute size ($p < 0.0001$,

repeated measures two-way ANOVA) and applied strain ($p < 0.0001$, repeated measures two-way ANOVA). Again, no significant differences in aqueous diffusivity were observed among quantification techniques (FCS vs. RICS) for a given experimental condition. Thus, in quantifying solute diffusivity within aqueous solutions and within agarose plugs, measurement by both FCS and RICS detection were both reproducible and highly consistent (Figure 5).

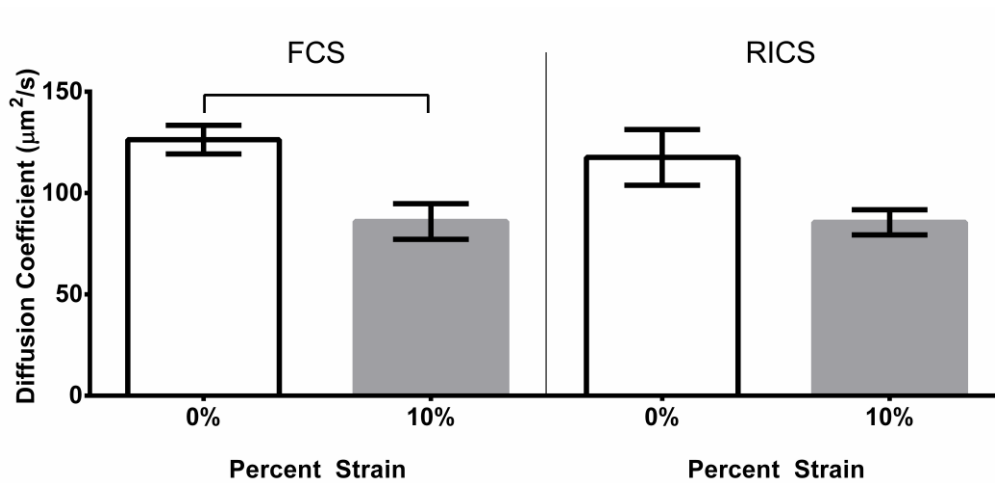


Figure 4: Diffusion coefficients of 3K dextran determined by FCS and RICS in 1% agarose at 0% and 10% compressive strain. Data reported as mean \pm SD. Bars indicate significant difference in diffusivity among uncompressed agarose plugs and plugs compressed to 10% strain ($p < 0.05$, paired t-test, $n = 5$ for each group). These data show that strain affects the diffusion coefficient of 3K dextran in 1% agarose, and while the diffusion coefficients obtained via RICS were not significantly different, there does seem to be a trend towards significance ($p=0.0535$).

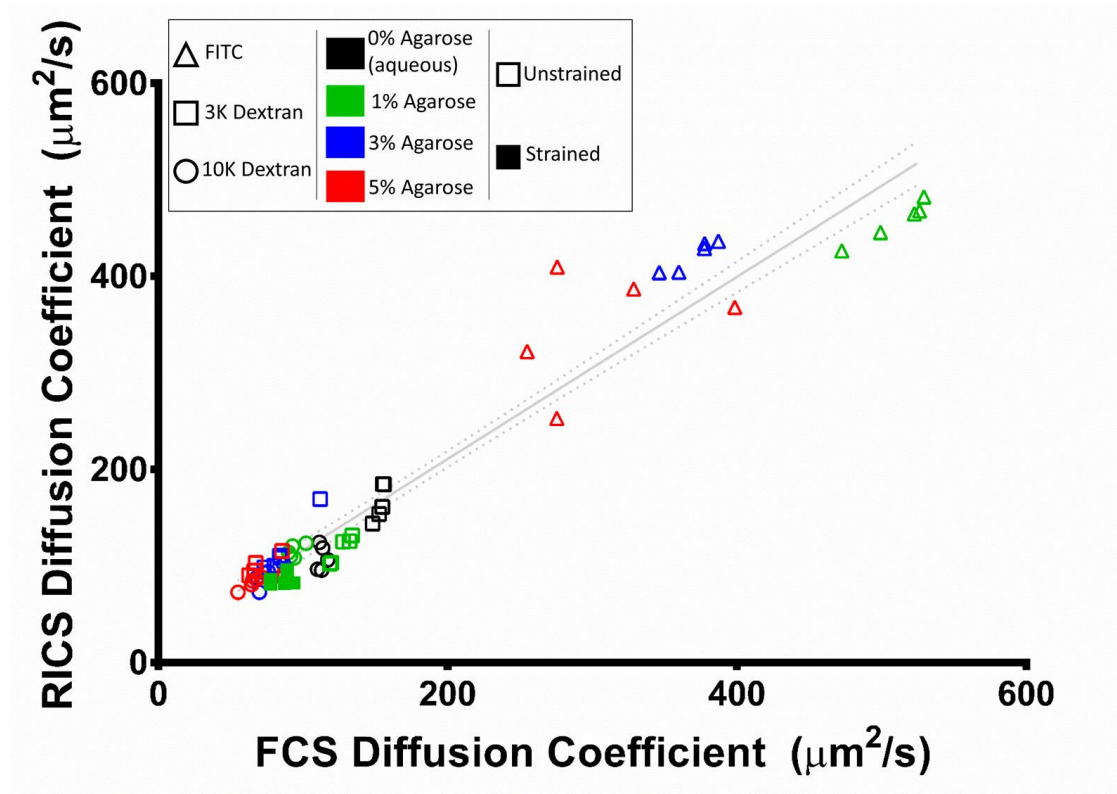


Figure 5: XY-scatter plot of paired FCS and RICS diffusivity measures for FITC, 3K dextran, and 10K dextran under the various experimental conditions tested (e.g. 0, 1, 3, and 5% agarose at 0% and 10% compressive strains). Individual data points for each tested condition are displayed. The linear regression line, as shown by the solid grey line was fit to the data set encompassing all conditions; $y = 0.9377x + 25.49$, 95% confidence intervals of the fit are shown by the dotted grey lines, $R^2 = 0.9469$, $p < 0.0001$. The slope and R^2 value being nearly equal to 1 demonstrates the repeatability of diffusivity measurements made by FCS and RICS.

3.2 Cartilage

Depth- (i.e. cartilage zone) and strain-dependent diffusivity of various nanomolar concentration fluorescent solutes were quantified in juvenile bovine articular cartilage plugs using FCS and RICS techniques. Quantification of diffusivity via both FCS and RICS demonstrated that axial compression (strain) significantly

influenced overall solute diffusivity (two-way ANOVA, FCS: $p=0.0001$, RICS: $p=0.0002$) (Figure 6). A trend towards decreased solute diffusivity was observed between the uncompressed and 10% strain conditions within each cartilage zone (data for 3K dextran is shown in Figure 6). However, no trends were apparent between higher levels of strain (20% or 30%) (Figure 6). The diffusivity of FITC and 3K Dextran were also compared in zonally matched cartilage samples. Two-way ANOVA of the FCS data revealed that cartilage zone significantly affected solute diffusivity ($p=0.0052$), while in the RICS data the trend was not significant ($p=0.1174$). Qualitatively, a difference between the diffusion coefficients of FITC and 3K dextran was observed in the superficial zone cartilage, but there were no obvious relationships for the middle and deep zones (Figure 7).

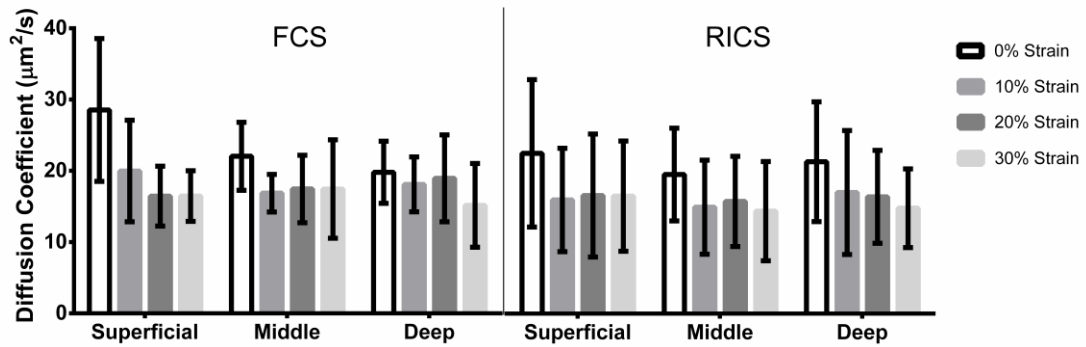


Figure 6: Diffusion coefficients of 3K dextran in the superficial, middle, and deep zones of bovine calf cartilage under 0, 10, 20, and 30% strains as determined by FCS (A) and RICS (B). While there was a trend toward decreasing 3k-dextran diffusivity with the application of 10% strain to the superficial layer under both techniques no significant differences were found between experimental groups ($p > 0.05$, One-way ANOVA, Tukey post-hoc and paired t-test, as applicable). Data reported as mean \pm SD ($n = 12$ for each group). While there were no significant differences in this data, there may be a slight decreasing trend in the diffusion coefficient of 3K dextran between 0% and 10% strain superficial zone cartilage.

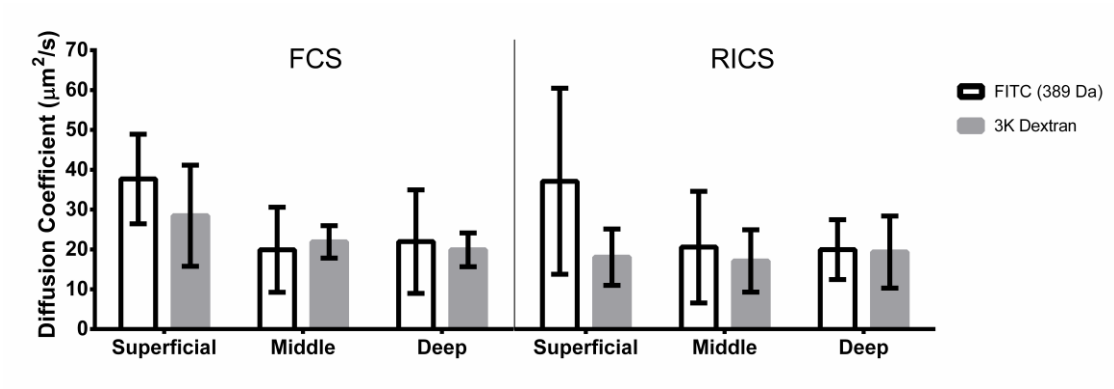


Figure 7: Diffusion coefficients of FITC and 3K dextran as determined by FCS (A) and RICS (B) in the superficial, middle, and deep zones of un-compressed bovine calf cartilage. No significant differences were found between experimental groups ($p > 0.05$, One-way ANOVA, Tukey post-hoc and paired t-test, as applicable). Data reported as mean \pm SD ($n = 6$ for each group). While there were no significant differences in this data, there may be a slight decreasing trend between the diffusion coefficients of FITC and 3K dextran in superficial zone cartilage; no trend is apparent in the middle and deep zone cartilage.

In general, it was observed that diffusivity measurements in cartilage were more variable than those in agarose gels (coefficient of variation ranged from 0.16 to 0.52 in cartilage, compared to 0.04 to 0.3 in agarose). This was presumably due to the increased heterogeneity of cartilage and the influence of this heterogeneity on data collection. Furthermore, the relationship between the paired diffusion coefficients quantified via FCS, versus those obtained by RICS in cartilage (Figure 8) was less robust than those observed within aqueous solution and agarose gels.

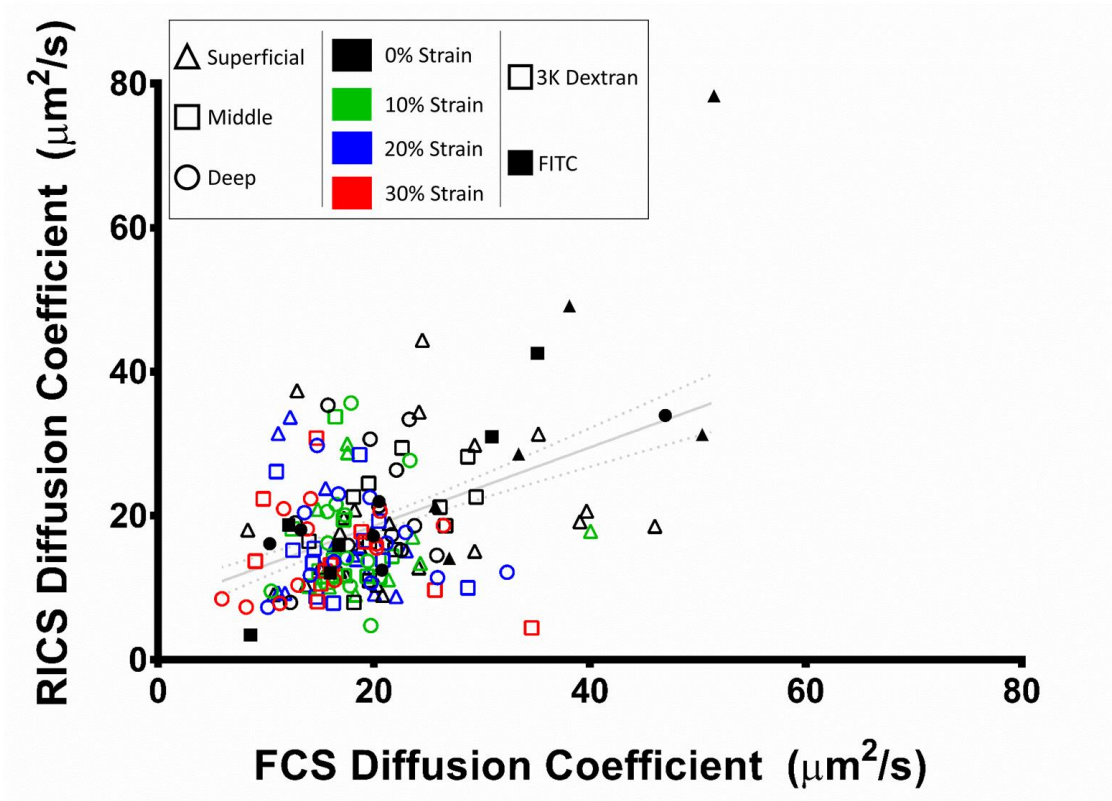


Figure 8: XY-scatter plot of diffusion coefficient values of 3K dextran and FITC in all cartilage zones, at all applied strains obtained by RICS versus those obtained by FCS. Data points denote the average diffusion coefficient across three locations within a sample. The linear regression line is shown by a solid grey line ($y = 0.5450x + 7.671$), with 95% confidence intervals shown by dotted grey lines. Significant correlation was found ($p < 0.0001$), $R^2 = 0.1820$. The low slope and R^2 values indicate low repeatability in quantifying the diffusion coefficient of 3K dextran in cartilage using FCS and RICS, perhaps due to the spatial heterogeneity in cartilage matrix structure.

Chapter 4

DISCUSSION

The avascular nature of cartilage requires that the transport of solutes (e.g. nutrients, waste, and signaling molecules) is facilitated through mechanical and/or thermodynamic processes within the joint. These processes are dependent upon the hierarchical structure of the cartilage, which changes throughout development, aging, and degeneration. Thus, solute diffusion, a critical regulator of articular cartilage homeostasis and pathology, has become an important area of research in studying/quantifying natural and disease state cartilage, as well as in assessing tissue engineered constructs [73, 2, 23, 13, 29, 24]. However, to date, the techniques used to quantify solute diffusivity in situ suffer from limitations such as invasiveness and spatial resolution. In this study, we demonstrated the utility of fluorescent correlation spectroscopy (FCS) and raster image correlation spectroscopy (RICS) as simple and minimally invasive ways to quantify solute diffusivity within porous, cartilaginous materials.

FCS and RICS represent valuable microscopy techniques for the study of diffusion in porous, hydrated materials. They allow for the direct microscale quantification of solute diffusivity in situ without having to rely on i) external perturbations to system under study, ii) the use of intense laser illumination, or iii) knowledge/assumptions regarding the specific system under observation. Instead, correlation spectroscopy techniques only require knowledge of easily obtained information regarding the optics and image collection parameters of the imaging system, such as the geometry of the PSF (FCS and RICS) and the dynamics and structure of the raster scanning imaging pattern (RICS). Subsequently, quantification

of solute diffusivity occurs through the simple application of autocorrelation analyses and the well-established Gaussian description of Brownian motion. Thus, correlation spectroscopy techniques are experimentally straightforward, and allow for the quantification of solute diffusivity in systems whose states are prohibitively difficult to define a priori.

The results of this study show that both FCS and RICS can be used to reliably quantify solute diffusion in porous media. The diffusion measurements obtained in agarose gels demonstrate the consistency and repeatability of diffusivity measurements obtained using both FCS and RICS, and are comparable to previously published data [74, 75, 76, 13]. Agarose gels represented an ideal system to test these techniques, since the properties of the porous media can be easily controlled and the resultant hydrogel structure is homogeneous [77, 78]. In contrast, articular cartilage is known to be structurally, compositionally, and mechanically heterogeneous, both throughout its depth [9, 79] and across its surface [10, 80, 5]. While we attempted to minimize heterogeneity in our samples by restricting the collection of cartilage plugs to the medial femoral condyles of similarly aged bovine calves, it is clear from the variability seen in our data that heterogeneity existed among the samples/analyses. Despite this variability, our results are comparable to a number of studies investigating zone- and strain-dependent diffusion coefficient values in cartilage using techniques such as solute desorption [81] and FRAP [9], further supporting the applicability of FCS and RICS for quantifying solute diffusion in articular cartilage.

Our data show, as expected, that solute size and matrix structure affect solute diffusion in hydrated porous media. In agarose gels, solute diffusivity decreased with increased solute size and increased gel concentration. This is intuitive, as one would

expect a higher concentration gel to be denser, have a shorter mean free path length, and thus further hinder solute diffusion. Zonally, cartilage location did not have an obvious effect on diffusivity, aside from the observation of a slightly higher diffusivity within the superficial zone. A similar trend has also been seen in previously published data [9], and could be attributed to the lower proteoglycan content in the superficial zone compared to the middle and deep zones [5]. While there are known matrix compositional and structural differences throughout the depth of the cartilage, heterogeneity also exists across the transverse aspect of the cartilage surface [8-12], which could further confound the ability to detect depth-wise differences through the tissue. Although all our samples came from the medial femoral condyles of a small number of similarly aged bovine calves, plugs were collected from across the entirety of the joint surface, thus the grouping of multiple plugs may be less appropriate due to intra-group heterogeneity caused by different sampling locations across the surface of the condyle, as well as inter-animal heterogeneity.

The demonstration of the utility of FCS and RICS in studying diffusion in biological tissue herein, and the simplicity and speed with which FCS and RICS techniques can be implemented on commercially available imaging platforms, suggests that these techniques are viable options for the in situ study of diffusion in a variety of situations. These include the direct characterization of developing, healthy, pathological, and treated cartilage tissues. As well as aiding in the direct, non-invasive testing of engineered and regenerated cartilaginous tissues. These techniques can also be readily adapted to the study of diffusion within a variety of musculoskeletal tissues, including tendon/ligament, muscle, bone, etc. However, it should be noted that the

planning of FCS and RICS data collection and analyses is an important component in the collection of robust diffusion data.

Specific concerns that need to be accounted for are: accurate calibration of the microscope's PSF, introduction of an appropriate fluorescent solute into the sample, and understanding the spatial limitations of each technique. Correctly establishing the geometry of the PSF can be achieved by imaging immobilized, point-source fluorescent beads (i.e. bead diameter smaller than the diffraction-limit resolution of the imaging device). However, this technique, while considered a gold-standard, requires specialized reconstruction and analysis software, and is oftentimes difficult to match to the experimental imaging conditions. Calibration of the PSF geometry based upon the use of a known diffusion standard is a quick, simple, and well-accepted method for PSF determination, but is not without limitations. Via the calibration technique, all diffusion values are calculated relative to the diffusivity specified for the calibration standard. In this manner, error in establishing absolute diffusivity is subject to the accurate adoption of a diffusion coefficient for the calibration solute. However, if all experiments are calibrated according to the same diffusion coefficient, the data remains internally consistent. In the present study, calibration was performed using fluorescein in aqueous solution at room temperature, for which a diffusion coefficient of $450 \mu\text{m}^2/\text{s}$ was established for system calibration [48, 49, 51]. We note that in using this specific reference standard the diffusion values we report for the various experimental groups are consistent with values previously reported in the literature [9, 13, 74-76]. In all optical observation systems, the choice of fluorescent solute must be made such that it has a minimal impact on the biological system being observed. This can be achieved easily using FCS and RICS, since only nanomolar concentrations of

solute are needed, and there exists a large number of non-reactive, photo-stable molecules (e.g. dyes, dextrans, proteins, etc.) appropriate for such analysis. Lastly, the spatial limitations of FCS and RICS must be considered in the construction and performance of imaging studies. For FCS analysis, the confocal observation region is restricted to a stationary observation volume (PSF) location, providing limited spatial knowledge unless the volume is subsequently repositioned with a given sample. For RICS, the observation region is larger than FCS, but is still restricted to $\sim 20 \mu\text{m}^2$. While these observation volumes may be small compared to the overall dimensions of articular cartilage, FCS and RICS do allow for the collection of diffusion measurements at resolutions unobtainable with other techniques, such as MRI and FRAP.

In the present study, only 3D isotropic diffusion of a single solute species was considered. The assumption of isotropic diffusion may be a simplification of solute diffusion within cartilage as collagen orientation varies throughout the thickness of the tissue [7, 29, 82, 83]. In the deep zone, collagen fiber orientation perpendicular to the articular surface could increase diffusive transport along this out-of-plane fiber direction. Conversely, superficial zone cartilage exhibits a collagen fiber orientation that is predominately transverse to articular surface, and could result in increased diffusive transport in this plane. Previous work has shown that such structural hierarchy can affect solute diffusion [40]. Thus, an anisotropic diffusion model may better describe the solute diffusion in articular cartilage. RICS has been used to quantify anisotropic diffusion in cardiomyocytes [84], and while beyond the scope of the present study, could similarly be used to quantify anisotropic diffusion in musculoskeletal tissue as well. Image correlation spectroscopy (ICS) techniques can

also be used model the kinetics of multiple diffusing species, either from separate emission channels or among similar emitting solutes with well-separated diffusivities [56, 59, 64]. However, for a given emission channel ICS is unable to discriminate amongst continuously varying populations or between populations with similar diffusion kinetics. The dextrans utilized in the study are polydisperse [74, 76], with molecular weight variances ranging up to ~50% of the nominal solute weight. Thus, reported diffusivities reflect the mean diffusivity of a broad population distribution, as opposed to a well-defined individual solute. Also, while the present study only considered diffusion at equilibrium, load-induced fluid flow is another mechanism for nutrient transport in articular cartilage. While RICS is restricted to diffusion measurements alone, FCS and other ICS techniques (such a spatiotemporal image correlation spectroscopy (STICS)) can potentially quantify convective solute transport within porous materials. FCS is able to measure high speed flows (up to 80 mm/s) [85-87] in various systems, and STICS has been applied to the study of convection across a range of slower speeds (between 0.1 and 2 $\mu\text{m/s}$) [59, 88, 89].

In conclusion, we have confirmed the ability of FCS, a well-established and commonly used aqueous diffusion characterization technique, to quantify solute diffusion within hydrogels and cartilage explants. We have also demonstrated that RICS, an image-based spectroscopy technique, can be used to quantify solute diffusion in hydrated, porous matrix environments with similar accuracy to FCS [47]. We have confirmed, using FCS and RICS, that solute diffusivity within hydrogels is dependent upon solute size, matrix composition, and applied strain. In cartilage, solute diffusivity is additionally dependent upon cartilage depth (zone). Together, FCS and RICS are microscopy-based techniques that are both simple to implement and provide

previously unachievable spatial resolution in quantifying solute diffusion in hydrogels and cartilage. Such micro-scale transport quantification techniques can be useful in examining micro-scale changes in solute-matrix interactions within biological tissue due to development, aging, disease, treatment, or regeneration, as well as within engineered materials and during the development and maturation of tissue constructs.

REFERENCES

1. Ateshian, G. a. (2009). The role of interstitial fluid pressurization in articular cartilage lubrication. *Journal of Biomechanics*, 42(9), 1163–76. <http://doi.org/10.1016/j.jbiomech.2009.04.040>
2. Greene, G. W., Zappone, B., S?derman, O., Topgaard, D., Rata, G., Zeng, H., & Israelachvili, J. N. (2010). Anisotropic dynamic changes in the pore network structure, fluid diffusion and fluid flow in articular cartilage under compression. *Biomaterials*, 31(12), 3117–3128. <http://doi.org/10.1016/j.biomaterials.2010.01.102>
3. Bonnevie, E. D., Baro, V. J., Wang, L., & Burris, D. L. (2012). Fluid load support during localized indentation of cartilage with a spherical probe. *Journal of Biomechanics*, 45(6), 1036–41. <http://doi.org/10.1016/j.jbiomech.2011.12.019>
4. Soltz, M. a, & Ateshian, G. a. (1998). Experimental verification and theoretical prediction of cartilage interstitial fluid pressurization at an impermeable contact interface in confined compression. *Journal of Biomechanics*, 31(10), 927–34. Retrieved from <http://www.ncbi.nlm.nih.gov/pubmed/9840758>
5. Mow, V. C., Ratcliffe, A., & Robin Poole, A. (1992). Cartilage and diarthrodial joints as paradigms for hierarchical materials and structures. *Biomaterials*, 13(2), 67–97. [http://doi.org/10.1016/0142-9612\(92\)90001-5](http://doi.org/10.1016/0142-9612(92)90001-5)
6. Armstrong, C. G., & Mow, V. C. (1982). Variations in the intrinsic mechanical properties of human articular cartilage with age, degeneration, and water content. *The Journal of Bone and Joint Surgery. American Volume*, 64(1), 88–94.
7. Halonen, K. S., Mononen, M. E., Jurvelin, J. S., Töyräs, J., & Korhonen, R. K. (2013). Importance of depth-wise distribution of collagen and proteoglycans in articular cartilage--a 3D finite element study of stresses and strains in human knee joint. *Journal of Biomechanics*, 46(6), 1184–92. <http://doi.org/10.1016/j.jbiomech.2012.12.025>
8. Shirazi, R., Shirazi-Adl, A., & Hurtig, M. (2008). Role of cartilage collagen fibrils networks in knee joint biomechanics under compression. *Journal of Biomechanics*, 41(16), 3340–3348. <http://doi.org/10.1016/j.jbiomech.2008.09.033>

9. Leddy, H. A., & Guilak, F. (2003). Site-specific molecular diffusion in articular cartilage measured using fluorescence recovery after photobleaching. *Annals of Biomedical Engineering*, 31(7), 753–760. <http://doi.org/10.1114/1.1581879>
10. Moore, a. C., & Burris, D. L. (2015). Tribological and material properties for cartilage of and throughout the bovine stifle: support for the altered joint kinematics hypothesis of osteoarthritis. *Osteoarthritis and Cartilage*, 23(1), 161–169. <http://doi.org/10.1016/j.joca.2014.09.021>
11. Korhonen, R. K., Julkunen, P., Rieppo, J., Lappalainen, R., Konttinen, Y. T., & Jurvelin, J. S. (2006). Collagen network of articular cartilage modulates fluid flow and mechanical stresses in chondrocyte. *Biomechanics and Modeling in Mechanobiology*, 5(2-3), 150–159. <http://doi.org/10.1007/s10237-006-0021-6>
12. Eckstein, F., Tieschky, M., Faber, S., Englmeier, K. H., & Reiser, M. (1999). Functional analysis of articular cartilage deformation, recovery, and fluid flow following dynamic exercise in vivo. *Anatomy and Embryology*, 200(4), 419–424. <http://doi.org/10.1007/s004290050291>
13. Leddy, H. a, Awad, H. a, & Guilak, F. (2004). Molecular diffusion in tissue-engineered cartilage constructs: effects of scaffold material, time, and culture conditions. *Journal of Biomedical Materials Research. Part B, Applied Biomaterials*, 70(2), 397–406. <http://doi.org/10.1002/jbm.b.30053>
14. Kisiday, J. D., Jin, M., DiMicco, M. A., Kurz, B., & Grodzinsky, A. J. (2004). Effects of dynamic compressive loading on chondrocyte biosynthesis in self-assembling peptide scaffolds. *Journal of Biomechanics*, 37(5), 595–604. <http://doi.org/10.1016/j.jbiomech.2003.10.005>
15. Serpooshan, V., Quinn, T. M., Muja, N., & Nazhat, S. N. (2013). Hydraulic permeability of multilayered collagen gel scaffolds under plastic compression-induced unidirectional fluid flow. *Acta Biomaterialia*, 9(1), 4673–4680. <http://doi.org/10.1016/j.actbio.2012.08.031>
16. Mauck, R. L., Soltz, M. a, Wang, C. C., Wong, D. D., Chao, P. H., Valhmu, W. B., ... Ateshian, G. a. (2000). Functional tissue engineering of articular cartilage through dynamic loading of chondrocyte-seeded agarose gels. *Journal of Biomechanical Engineering*, 122(3), 252–260. <http://doi.org/10.1115/1.429656>

17. Hoenig, E., Leicht, U., Winkler, T., Mielke, G., Beck, K., Peters, F., ... Morlock, M. M. (2013). Mechanical Properties of Native and Tissue-Engineered Cartilage Depend on Carrier Permeability: A Bioreactor Study. *Tissue Engineering Part A*, *19*(13-14), 1534–1542. <http://doi.org/10.1089/ten.tea.2012.0538>
18. Buschmann, M. D., Kim, Y. J., Wong, M., Frank, E., Hunziker, E. B., & Grodzinsky, A. J. (1999). Stimulation of aggrecan synthesis in cartilage explants by cyclic loading is localized to regions of high interstitial fluid flow. *Archives of Biochemistry and Biophysics*, *366*(1), 1–7. <http://doi.org/10.1006/abbi.1999.1197>
19. Davisson, T., Kunig, S., Chen, A., Sah, R., & Ratcliffe, A. (2002). Static and dynamic compression modulate matrix metabolism in tissue engineered cartilage. *Journal of Orthopaedic Research*, *20*, 842–8.
20. Kim, Y. J., Bonassar, L. J., & Grodzinsky, A. J. (1995). The role of cartilage streaming potential, fluid flow and pressure in the stimulation of chondrocyte biosynthesis during dynamic compression. *Journal of Biomechanics*, *28*(9), 1055–1066. [http://doi.org/10.1016/0021-9290\(94\)00159-2](http://doi.org/10.1016/0021-9290(94)00159-2)
21. Arkill, K. P., & Winlove, C. P. (2006). Fatty acid transport in articular cartilage. *Archives of Biochemistry and Biophysics*, *456*(1), 71–78. <http://doi.org/10.1016/j.abi.2006.09.014>
22. Poole, K., Herget, R., Lapatsina, L., Ngo, H.-D., & Lewin, G. R. (2014). Tuning Piezo ion channels to detect molecular-scale movements relevant for fine touch. *Nature Communications*, *5*, 3520. <http://doi.org/10.1038/ncomms4520>
23. Crema, M. D., Roemer, F. W., Marra, M. D., Burstein, D., Gold, G. E., Eckstein, F., ... Guermazi, A. (2011). Articular cartilage in the knee: current MR imaging techniques and applications in clinical practice and research. *Radiographics*, *31*(1), 37–61. <http://doi.org/10.1148/rg.311105084>
24. Ukai, T., Sato, M., Yamashita, T., Imai, Y., Mitani, G., Takagaki, T., ... Mochida, J. (2015). Diffusion tensor imaging can detect the early stages of cartilage damage: a comparison study. *BMC Musculoskeletal Disorders*, *16*, 35. <http://doi.org/10.1186/s12891-015-0499-0>

25. de Visser, S. K., Crawford, R. W., & Pope, J. M. (2008). Structural adaptations in compressed articular cartilage measured by diffusion tensor imaging. *Osteoarthritis and Cartilage*, *16*(1), 83–89. <http://doi.org/10.1016/j.joca.2007.05.013>
26. Raya, J. G., Arnoldi, A. P., Weber, D. L., Filidoro, L., Dietrich, O., Adam-Neumair, S., ... Glaser, C. (2011). Ultra-high field diffusion tensor imaging of articular cartilage correlated with histology and scanning electron microscopy. *Magnetic Resonance Materials in Physics, Biology and Medicine*, *24*(4), 247–258. <http://doi.org/10.1007/s10334-011-0259-6>
27. Raya, J. G., Horng, A., Dietrich, O., Krasnokutsky, S., Beltran, L. S., Storey, P., ... Glaser, C. (2012). Articular cartilage: in vivo diffusion-tensor imaging. *Radiology*, *262*(2), 550–559. <http://doi.org/10.1148/radiol.11110821>
28. Deng, X., Farley, M., Nieminen, M. T., Gray, M., & Burstein, D. (2007). Diffusion tensor imaging of native and degenerated human articular cartilage. *Magnetic Resonance Imaging*, *25*(2), 168–171. <http://doi.org/10.1016/j.mri.2006.10.015>
29. Meder, R., de Visser, S. K., Bowden, J. C., Bostrom, T., & Pope, J. M. (2006). Diffusion tensor imaging of articular cartilage as a measure of tissue microstructure. *Osteoarthritis and Cartilage*, *14*(9), 875–881. <http://doi.org/10.1016/j.joca.2006.03.002>
30. Filidoro, L., Dietrich, O., Weber, J., Rauch, E., Oerther, T., Wick, M., ... Glaser, C. (2005). High-resolution diffusion tensor imaging of human patellar cartilage: Feasibility and preliminary findings. *Magnetic Resonance in Medicine*, *53*(5), 993–998. <http://doi.org/10.1002/mrm.20469>
31. Burstein, D., Gray, M. L., Hartman, A. L., Gipe, R., & Foy, B. D. (1993). Diffusion of small solutes in cartilage as measured by nuclear magnetic resonance (NMR) spectroscopy and imaging. *Journal of Orthopaedic Research*, *11*(4), 465–478. <http://doi.org/10.1002/jor.1100110402>
32. Knauss, R., Schiller, J., Fleischer, G., K??rger, J., & Arnold, K. (1999). Self-diffusion of water in cartilage and cartilage components as studied by pulsed field gradient NMR. *Magnetic Resonance in Medicine*, *41*(2), 285–292. [http://doi.org/10.1002/\(SICI\)1522-2594\(199902\)41:2<285::AID-MRM11>3.0.CO;2-3](http://doi.org/10.1002/(SICI)1522-2594(199902)41:2<285::AID-MRM11>3.0.CO;2-3)

33. Ngwa, W., Geier, O., Stallmach, F., Naji, L., Schiller, J., & Arnold, K. (2002). Cation diffusion in cartilage measured by pulsed field gradient NMR. *European Biophysics Journal*, *31*(1), 73–80.
<http://doi.org/10.1007/s002490100184>
34. Trampel, R., Schiller, J., Naji, L., Stallmach, F., K?rger, J., & Arnold, K. (2002). Self-diffusion of polymers in cartilage as studied by pulsed field gradient NMR. *Biophysical Chemistry*, *97*(2-3), 251–260.
[http://doi.org/10.1016/S0301-4622\(02\)00078-9](http://doi.org/10.1016/S0301-4622(02)00078-9)
35. Fischer, A. E., Carpenter, T. A., Tyler, J. A., & Hall, L. D. (1995). Visualisation of mass transport of small organic molecules and metal ions through articular cartilage by magnetic resonance imaging. *Magnetic Resonance Imaging*, *13*(6), 819–26. Retrieved from
<http://www.ncbi.nlm.nih.gov/pubmed/8544653>
36. Fischer, A. E., & Hall, L. D. (1996). Visualization of the diffusion of metal ions and organic molecules by magnetic resonance imaging of water. *Magnetic Resonance Imaging*, *14*(7-8), 779–783.
[http://doi.org/10.1016/S0730-725X\(96\)00163-4](http://doi.org/10.1016/S0730-725X(96)00163-4)
37. Jones, C. W., Smolinski, D., Willers, C., Yates, P. J., Keogh, A., Fick, D., ... Zheng, M. H. (2007). Laser scanning confocal arthroscopy of a fresh cadaveric knee joint. *Osteoarthritis and Cartilage*, *15*(12), 1388–1396.
<http://doi.org/10.1016/j.joca.2007.05.003>
38. Fomby, P., & Cherlin, A. J. (2011). Identification of cartilage injury using multiphoton microscopy, *72*(2), 181–204.
<http://doi.org/10.1038/nature13314.A>
39. Menashe, L., Hirko, K., Losina, E., Kloppenburg, M., Zhang, W., Li, L., & Hunter, D. J. (2012). The diagnostic performance of MRI in osteoarthritis: A systematic review and meta-analysis. *Osteoarthritis and Cartilage*, *20*(1), 13–21. <http://doi.org/10.1016/j.joca.2011.10.003>
40. Leddy, H. a, & Guilak, F. (2008). Site-specific effects of compression on macromolecular diffusion in articular cartilage. *Biophysical Journal*, *95*(10), 4890–5. <http://doi.org/10.1529/biophysj.108.137752>
41. Pan, J., Zhou, X., Li, W., Novotny, J. E., Doty, S. B., & Wang, L. (2009). In situ measurement of transport between subchondral bone and articular cartilage. *Journal of Orthopaedic Research*, *27*(10), 1347–1352.
<http://doi.org/10.1002/jor.20883>

42. Pan, J., Wang, B., Li, W., Zhou, X., Scherr, T., Yang, Y., ... Wang, L. (2012). Elevated cross-talk between subchondral bone and cartilage in osteoarthritic joints. *Bone*, *51*(2), 212–217. <http://doi.org/10.1016/j.bone.2011.11.030>
43. Williams, R. M., Zipfel, W. R., Tinsley, M. L., & Farnum, C. E. (2007). Solute transport in growth plate cartilage: in vitro and in vivo. *Biophysical Journal*, *93*(3), 1039–50. <http://doi.org/10.1529/biophysj.106.097675>
44. Soumpasis, D. M. (1983). Theoretical analysis of fluorescence photobleaching recovery experiments. *Biophysical Journal*, *41*(1), 95–97. [http://doi.org/10.1016/S0006-3495\(83\)84410-5](http://doi.org/10.1016/S0006-3495(83)84410-5)
45. Castle, B. T., Howard, S. A., & Odde, D. J. (2011). Assessment of transport mechanisms underlying the bicoid morphogen gradient. *Cellular and Molecular Bioengineering*, *4*(1), 116–121. <http://doi.org/10.1007/s12195-010-0157-4>
46. Dobrucki, J. W., Feret, D., & Noatynska, A. (2007). Scattering of exciting light by live cells in fluorescence confocal imaging: phototoxic effects and relevance for FRAP studies. *Biophysical Journal*, *93*(5), 1778–1786. <http://doi.org/10.1529/biophysj.106.096636>
47. Lee, J. I., Sato, M., Ushida, K., & Mochida, J. (2011). Measurement of diffusion in articular cartilage using fluorescence correlation spectroscopy. *BMC Biotechnology*, *11*(1), 19. <http://doi.org/10.1186/1472-6750-11-19>
48. Digman, M. a., Brown, C. M., Sengupta, P., Wiseman, P. W., Horwitz, A. R., & Gratton, E. (2005). Measuring fast dynamics in solutions and cells with a laser scanning microscope. *Biophysical Journal*, *89*(2), 1317–27. <http://doi.org/10.1529/biophysj.105.062836>
49. Digman, M. a, Sengupta, P., Wiseman, P. W., Brown, C. M., Horwitz, A. R., & Gratton, E. (2005). Fluctuation correlation spectroscopy with a laser-scanning microscope: exploiting the hidden time structure. *Biophysical Journal*, *88*(5), L33–6. <http://doi.org/10.1529/biophysj.105.061788>
50. Elson, E. L., & Magde, D. (1974). Fluorescence correlation spectroscopy. I. Conceptual basis and theory. *Biopolymers*, *13*(1), 1–27. <http://doi.org/10.1002/bip.1974.360130102>

51. Brown, C. M., Dalal, R. B., Hebert, B., Digman, M. a, Horwitz, a R., & Gratton, E. (2008). Raster image correlation spectroscopy (RICS) for measuring fast protein dynamics and concentrations with a commercial laser scanning confocal microscope. *Journal of Microscopy*, 229(Pt 1), 78–91. <http://doi.org/10.1111/j.1365-2818.2007.01871.x>
52. Hendrix, J., & Lamb, D. C. (2013). Pulsed interleaved excitation: principles and applications. *Methods in Enzymology*, 518, 205–43. <http://doi.org/10.1016/B978-0-12-388422-0.00009-1>
53. Magde, D. (1972). *Letters* 11, 29(September), 705–708.
54. Magde, D., Elson, E. L., & Webb, W. W. (1974). Fluorescence Correlation Spectroscopy. II. An Experimental Realization. *Biopolymers*, 13, 29–61. <http://doi.org/10.1002/bip.1974.360130103>
55. Krichevsky, O. (2002). Fluorescence correlation spectroscopy : the technique. *Reports on Progress in Physics*, 65, 251–297.
56. Haustein, E., & Schwille, P. (2007). Fluorescence correlation spectroscopy: novel variations of an established technique. *Annual Review of Biophysics and Biomolecular Structure*, 36, 151–69. <http://doi.org/10.1146/annurev.biophys.36.040306.132612>
57. Gielen, E., Smisdom, N., vandeVen, M., De Clercq, B., Gratton, E., Digman, M., ... Ameloot, M. (2009). Measuring diffusion of lipid-like probes in artificial and natural membranes by raster image correlation spectroscopy (RICS): use of a commercial laser-scanning microscope with analog detection. *Langmuir : The ACS Journal of Surfaces and Colloids*, 25(9), 5209–18. <http://doi.org/10.1021/la8040538>
58. Ranjit, S., Lanzano, L., & Gratton, E. (2014). Mapping Diffusion in a Living Cell via the Phasor Approach. *Biophysical Journal*, 107(12), 2775–2785. <http://doi.org/10.1016/j.bpj.2014.08.041>
59. Kolin, D. L., & Wiseman, P. W. (2007). Advances in image correlation spectroscopy: measuring number densities, aggregation states, and dynamics of fluorescently labeled macromolecules in cells. *Cell Biochemistry and Biophysics*, 49(3), 141–64. <http://doi.org/10.1007/s12013-007-9000-5>

60. Seksek, O., & Verkman, a S. (1997). Translational diffusion of macromolecule-size solutes in cytoplasm and nucleus: Evidence for diffusion-restricting compartments without sieving. *Biophysical Journal*, 72(2), Tu372–Tu372. <http://doi.org/10.1083/jcb.138.1.131>
61. Culbertson, C. (2002). Diffusion coefficient measurements in microfluidic devices. *Talanta*, 56(2), 365–373. [http://doi.org/10.1016/S0039-9140\(01\)00602-6](http://doi.org/10.1016/S0039-9140(01)00602-6)
62. Rani, S. A., Pitts, B., & Stewart, P. S. (2005). Rapid diffusion of fluorescent tracers into Staphylococcus epidermidis biofilms visualized by time lapse microscopy. *Antimicrobial Agents and Chemotherapy*, 49(2), 728–732. <http://doi.org/10.1128/AAC.49.2.728-732.2005>
63. Casalini, T., Salvalaglio, M., Perale, G., Masi, M., & Cavallotti, C. (2011). Diffusion and aggregation of sodium fluorescein in aqueous solutions. *Journal of Physical Chemistry B*, 115(44), 12896–12904. <http://doi.org/10.1021/jp207459k>
64. Digman, M. a, & Gratton, E. (2011). Lessons in fluctuation correlation spectroscopy. *Annual Review of Physical Chemistry*, 62, 645–68. <http://doi.org/10.1146/annurev-physchem-032210-103424>
65. Digman, M. A., & Gratton, E. (2012). Scanning image correlation spectroscopy. *BioEssays*, 34(5), 377–385. <http://doi.org/10.1002/bies.201100118>
66. Wiseman, P. W. (2013). Image correlation spectroscopy: mapping correlations in space, time, and reciprocal space. *Methods in enzymology* (1st ed., Vol. 518). Elsevier Inc. <http://doi.org/10.1016/B978-0-12-388422-0.00010-8>
67. Aragón, S. R., & Pecora, R. (1975). Fluorescence correlation spectroscopy and Brownian rotational diffusion. *Biopolymers*, 14, 119–137. <http://doi.org/10.1002/bip.1975.360140110>
68. Elson, E. L. (2013). Brief introduction to fluorescence correlation spectroscopy. *Methods in Enzymology*, 518, 11–41. <http://doi.org/10.1016/B978-0-12-388422-0.00002-9>
69. Gröner, N., Capoulade, J., Cremer, C., & Wachsmuth, M. (2010). Measuring and imaging diffusion with multiple scan speed image correlation spectroscopy. *Optics Express*, 18(20), 21225–21237. <http://doi.org/10.1364/OE.18.021225>

70. Hamrang, Z., Pluen, A., Zindy, E., & Clarke, D. (2012). Raster Image Correlation Spectroscopy as a Novel Tool for the Quantitative Assessment of Protein Diffusional Behaviour in Solution, *101*(6), 2082–2093. <http://doi.org/10.1002/jps>
71. Moens, P. D. J., Gratton, E., & Salvemini, I. L. (2011). Fluorescence correlation spectroscopy, raster image correlation spectroscopy, and number and brightness on a commercial confocal laser scanning microscope with analog detectors (Nikon C1). *Microscopy Research and Technique*, *74*(4), 377–88. <http://doi.org/10.1002/jemt.20919>
72. Rossow, M., Sasaki, J., Digman, M., & Gratton, E. (2010). Raster image correlation spectroscopy in live cells. *Nature Protocols*. Retrieved from <http://www.nature.com/nprot/journal/v5/n11/abs/nprot.2010.122.html>
73. Raya, J. G., Melkus, G., Adam-Neumair, S., Dietrich, O., Mützel, E., Reiser, M. F., ... Glaser, C. (2013). Diffusion-tensor imaging of human articular cartilage specimens with early signs of cartilage damage. *Radiology*, *266*(3), 831–841. <http://doi.org/10.1148/radiol.12120954>
74. Pluen, a, Netti, P. a, Jain, R. K., & Berk, D. a. (1999). Diffusion of macromolecules in agarose gels: comparison of linear and globular configurations. *Biophysical Journal*, *77*(1), 542–552. [http://doi.org/10.1016/S0006-3495\(99\)76911-0](http://doi.org/10.1016/S0006-3495(99)76911-0)
75. Labille, J., Fatin-rouge, N., & Buffle, J. (2007). Local and Average Diffusion of Nanosolutes in Agarose Gel : The Effect of the Gel / Solution Interface Structure Local and Average Diffusion of Nanosolutes in Agarose Gel : The Effect of the Gel / Solution Interface Structure. *Society*, (12), 2083–2090. <http://doi.org/10.1021/la0611155>
76. Nicholson, C., & Tao, L. (1993). Hindered diffusion of high molecular weight compounds in brain extracellular microenvironment measured with integrative optical imaging. *Biophysical Journal*, *65*(6), 2277–2290. [http://doi.org/10.1016/S0006-3495\(93\)81324-9](http://doi.org/10.1016/S0006-3495(93)81324-9)
77. Buckley, C. T., Thorpe, S. D., & Kelly, D. J. (2009). Engineering of large cartilaginous tissues through the use of microchanneled hydrogels and rotational culture. *Tissue Engineering. Part A*, *15*(11), 3213–20. <http://doi.org/10.1089/ten.TEA.2008.0531>

78. Mesallati, T., Buckley, C. T., Nagel, T., & Kelly, D. J. (2013). Scaffold architecture determines chondrocyte response to externally applied dynamic compression. *Biomechanics and Modeling in Mechanobiology*, 12(5), 889–899. <http://doi.org/10.1007/s10237-012-0451-2>
79. Gao, L. L., Zhang, C. Q., Dong, L. M., & Jia, Y. W. (2012). Description of depth-dependent nonlinear viscoelastic behavior for articular cartilage in unconfined compression. *Materials Science and Engineering C*, 32(2), 119–125. <http://doi.org/10.1016/j.msec.2011.10.005>
80. Federico, S., & Herzog, W. (2008). On the anisotropy and inhomogeneity of permeability in articular cartilage. *Biomechanics and Modeling in Mechanobiology*, 7(5), 367–378. <http://doi.org/10.1007/s10237-007-0091-0>
81. Quinn, T. M., Kocian, P., & Meister, J. J. (2000). Static compression is associated with decreased diffusivity of dextrans in cartilage explants. *Archives of Biochemistry and Biophysics*, 384(2), 327–34. <http://doi.org/10.1006/abbi.2000.2077>
82. Jeffery, A., Blunn, G., Archer, C., & Bentley, G. (1991). Three-dimensional collagen architecture in bovine articular cartilage. *Journal of Bone and Joint Surgery*, 73(5), 795–801.
83. Thambyah, A., & Broom, N. (2006). Micro-anatomical response of cartilage-on-bone to compression: Mechanisms of deformation within and beyond the directly loaded matrix. *Journal of Anatomy*, 209(5), 611–622. <http://doi.org/10.1111/j.1469-7580.2006.00646.x>
84. Vendelin, M., & Birkedal, R. (2008). Anisotropic diffusion of fluorescently labeled ATP in rat cardiomyocytes determined by raster image correlation spectroscopy. *American Journal of Physiology. Cell Physiology*, 1302–1315. <http://doi.org/10.1152/ajpcell.00313.2008>.
85. Lumma, D., Best, a, Gansen, a, Feuillebois, F., Rädler, J. O., & Vinogradova, O. I. (2003). Flow profile near a wall measured by double-focus fluorescence cross-correlation. *Physical Review. E, Statistical, Nonlinear, and Soft Matter Physics*, 67(5 Pt 2), 056313. <http://doi.org/10.1103/PhysRevE.67.056313>
86. Kuricheti, K. K., Buschmann, V., & Weston, K. D. (2004). Application of fluorescence correlation spectroscopy for velocity imaging in microfluidic devices. *Applied Spectroscopy*, 58(10), 1180–1186. <http://doi.org/10.1366/0003702042335957>

87. Brister, P. C., Kuricheti, K. K., Buschmann, V., & Weston, K. D. (2005). Fluorescence correlation spectroscopy for flow rate imaging and monitoring--optimization, limitations and artifacts. *Lab on a Chip*, 5(7), 785–791. <http://doi.org/10.1039/b500129c>
88. Bove, J., Vaillancourt, B., Kroeger, J., Hepler, P. K., Wiseman, P. W., & Geitmann, A. (2008). Magnitude and direction of vesicle dynamics in growing pollen tubes using spatiotemporal image correlation spectroscopy and fluorescence recovery after photobleaching. *Plant Physiology*, 147(4), 1646–1658. <http://doi.org/10.1104/pp.108.120212>
89. Hebert, B., Costantino, S., & Wiseman, P. W. (2005). Spatiotemporal Image Correlation Spectroscopy (STICS) Theory, Verification, and Application to Protein Velocity Mapping in Living CHO Cells. *Biophysical Journal*, 88(5), 3601–3614. <http://doi.org/10.1529/biophysj.104.054874>

Appendix A

SUPPLEMENTAL INFORMATION

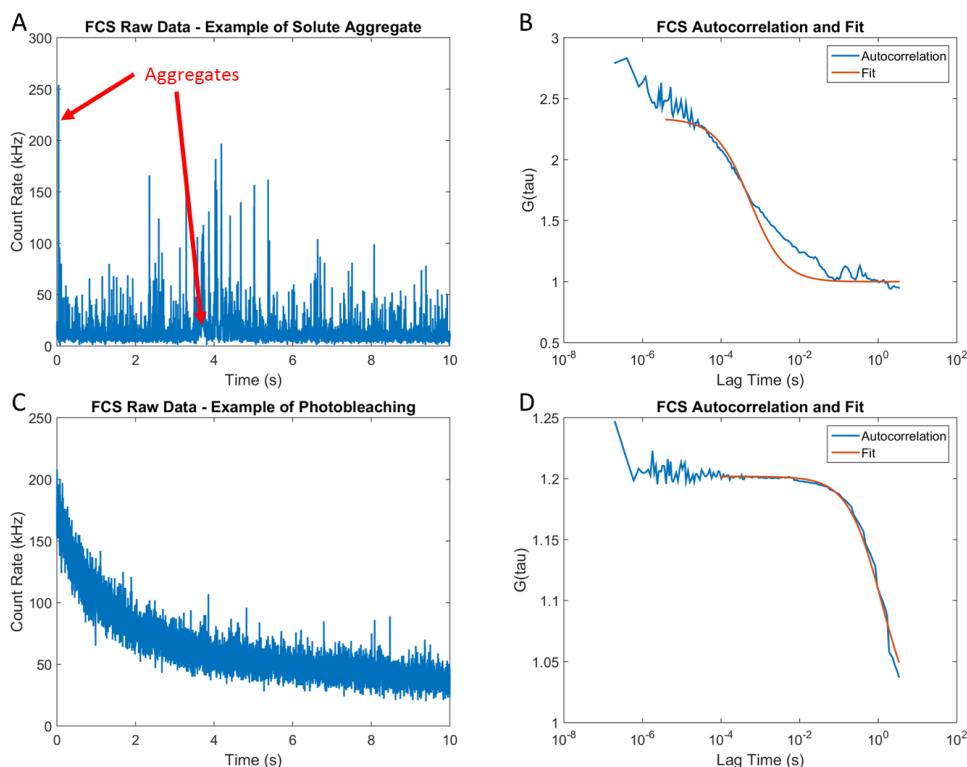


Figure A.1: **(A)** Example of a 10-second FCS trial that has spurious peaks much higher than the rest of the dataset. Such peaks are typically indicative of an aggregate of fluorescent solute particles, and the 10-second trial in which such peaks occurred were excluded from the diffusion analysis. **(B)** The autocorrelation and model fit of representative data containing an aggregate of fluorescent particles data. The presence of the aggregate results in a second, superimposed “hump” in the autocorrelation, indicative of a second solute species being present in the observation volume. **(C)** Example of a 10-second FCS trial in which photobleaching of the fluorescent particles (typically of an immobile fraction) has occurred. The photobleaching effect manifests in an exponentially decaying photon count rate. Any 10-second trials in which photobleaching effects were seen were removed from the diffusion analysis. **(D)** The autocorrelation and model fit of representative data exhibiting time-dependent photobleaching. Notice the drastically delayed decay time due to the contribution of the slow photobleaching kinetics.

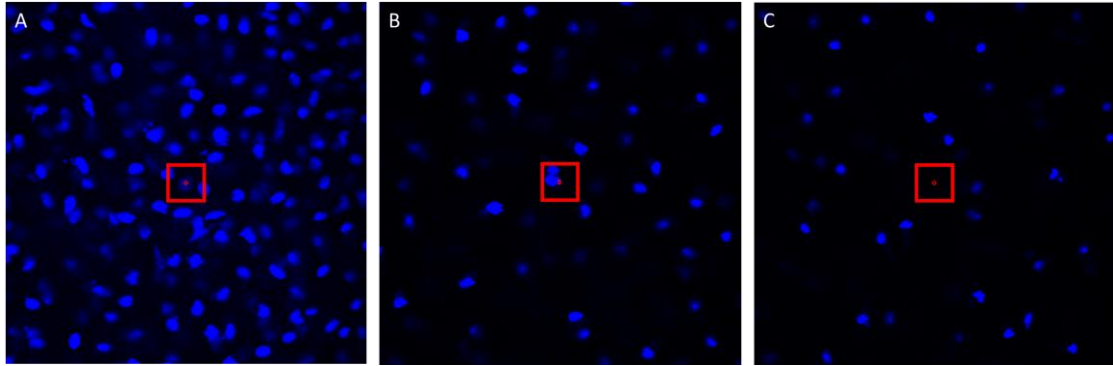


Figure A.2: These are images of DAPI-stained cell nuclei in the superficial (**A**), middle (**B**), and deep (**C**) zones of a cartilage plug. These images were taken at 20X magnification, under 405 nm laser light exposure. These images demonstrate the heterogeneity in cellularity between the superficial and middle and deep zones. When performing FCS and RICS analyses, we avoided taking diffusion measurements within a cell. However, due to the increased cellularity in the superficial zone, this was not always achievable for every sample. The red boxes and red dots represent the sizes of the RICS and FCS observation regions, respectively.